Competing crystal structures in $La_{0.5}Ca_{0.5}MnO_3$: Conventional charge order versus Zener polarons

C. H. Patterson
Department of Physics and Centre for Scientific Computation, University of Dublin, Trinity College, Dublin 2, Ireland
(Received 11 May 2005; published 18 August 2005)

Equilibrium crystal structures for $La_{0.5}Ca_{0.5}MnO_3$ have been calculated using hybrid Hartree-Fock and density functional methods. Two distinct ground states with either conventional checkerboard charge ordering, in which Mn ions have formal valence 3 or 4, or Zener polaron formation, in which each Mn ion has valence 3.5, are found depending on the proportion of Hartree-Fock exchange used. These structures correspond to those identified by various experiments and they differ by small displacements of key oxygen ions.

DOI: 10.1103/PhysRevB.72.085125 PACS number(s): 71.27.+a, 75.30.Et, 75.47.Lx, 75.10.−b

I. INTRODUCTION

Low temperature charge ordering (CO) transitions in manganites such as $La_{1-x}Ca_xMnO_3$ are generic for doping in the range $0.4<x<0.9$.[1–8] They are observed as commensurate or incommensurate changes in unit cell dimension parallel to the crystallographic **b** axis.[9] Commensurate structures are found when x is a rational fraction such as 1/2, 2/3 or 3/4. Half-doped manganites, $A_{0.5}B_{0.5}MnO_3$ with A=La, Nd, Pr and B=Ca, Sr, have been widely studied as the CO phase is believed to consist of a checkerboard (CB) pattern of Mn^{3+} and Mn^{4+} ions[2,10,11] in which Mn^{3+} ions are Jahn-Teller (JT) distorted while Mn^{4+} ions are not. However, there is evidence from unrestricted Hartree-Fock calculations (UHF)[12,13] on $La_{0.5}Ca_{0.5}MnO_3$ for a Zener polaron (ZP) electronic structure[14] in which all Mn ions have a valence of 3.5 and a recent single-crystal neutron scattering study found a ZP crystal structure for $Pr_{0.60}Ca_{0.40}MnO_3$ (Ref. 15) where all Mn ions have an intermediate JT distortion. The ZP electronic structure is also found in cluster configuration interaction (CI) calculations[16,17] and model Hamiltonian calculations[18] show that both CB and ZP states are possible around $x=1/2$. There is conflicting experimental evidence from resonant XRD experiments[19] for a CB CO pattern in $Pr_{0.60}Ca_{0.40}MnO_3$ and a recent refinement of the structure of $Pr_{0.5}Ca_{0.5}MnO_3$ using high resolution x-ray and neutron powder data which favored a CB structure.[20] Both CB and ZP phases have been proposed to exist in a phase diagram for half-doped manganites in which the tolerance ratio for the rare earth and alkaline earth ions is varied.[21] Powder neutron and x-ray diffraction experiments[2,22] and x-ray absorption near edge structure (XANES)[23,24] and resonant x-ray diffraction (RXD)[25] support a CB CO picture for $La_{0.5}Ca_{0.5}MnO_3$.

In this paper we use hybrid Hartree-Fock/density functional theory *ab initio* energy minimization methods and show that the ground state CO crystal structure switches between CB and ZP as the percentage of Hartree-Fock (HF) exchange is varied. These two states are therefore similar in energy and the actual ground state may depend on specific A and B ions,[21] or even sample preparation, history, and ambient conditions. The predominant difference in charge populations of the two states is in charge on O ions rather than Mn ions and so CO may be associated with O ions rather than Mn ions. Furthermore, we find that the lowest energy structure for either CO pattern has a different space group from those proposed for the CB (Ref. 2) or ZP (Ref. 15) structures. The structure that we find has modulations of Mn and O ion positions about ideal perovskite positions which are parallel to **ab** planes and transverse to the **b** axis and are similar to those observed in layered[4,5] and simple doped manganites.[1–3,6–8] A TA phonon softening mechanism for the CO transition would explain the observation of incommensurate order with wave vector $\mathbf{q}=(1-x)\mathbf{b}^*$ (Ref. 9) and may also be relevant to colossal magnetoresistance (CMR) phases of manganites where diffuse satellites in x-ray scattering have been observed[26,27] and attributed to polarons with transverse displacements of ions[27] similar to those in Fig. 1(a).

Structure optimizations were performed using the CRYSTAL program.[28] A $\sqrt{2}\times2\sqrt{2}\times2$ unit cell (Fig. 1) containing eight formula units with ferromagnetic (FM) order was used for optimizations while total energies of A and CE-type magnetically ordered structures were compared using $2\sqrt{2}\times2\sqrt{2}\times2$ unit cells. A single force evaluation was carried out for CE-type magnetic order for a structure which had been optimized with FM magnetic order in order to estimate the importance of magnetoelastic effects on the crystal structure; these were found to be small. No simultaneous relaxation of unit cell dimensions was performed as the calculations are expensive in computer time; unit cell dimensions were taken from experiment[2] ($a=5.4763$ Å, $b=10.8932$ Å, $c=7.5247$ Å). Structure optimizations were performed for 60%, 80%, and 100% HF exchange (the latter is simply a UHF wave function); both the 60% and 80% calculations resulted in CB CO for all space groups investigated while the UHF calculation resulted in ZP CO structures. Initial atomic configurations were taken from Table II in Ref. 2 ($P112_1/m$ symmetry) or were generated by hand. As noted by Daoud-Aladine and co-workers,[15] the isotropy subgroups of the parent high temperature $Pbnm$ phase that have a doubled unit cell along the **b** axis are $P11m$, $P2_1nm$, $P112_1/m$, $P112_1/b$, $P2_1nb$, and $P11b$. The relevant isotropy subgroups for ZP CO are $P2_1nm$ and $P11m$ and for CB CO they are $P112_1/m$ and $P11m$.

Hessian matrices for energy minimized CB or ZP CO structures with these space groups had at least one negative eigenvalue, which indicates that they are saddle points on the

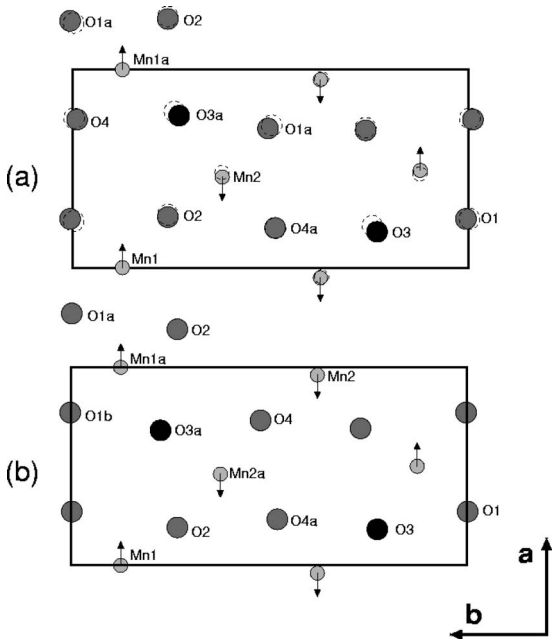

FIG. 1. **ab** plane atomic positions for $La_{0.5}Ca_{0.5}MnO_3$ shown to scale. (a) $Pn2_1m$ structure. Mn ion positions in the ZP state (Table I) are indicated by small circles, O^{2-} ions by shaded circles and O^- ions in the ZP state by a filled circle. Mn and O ion positions in the checkerboard state (Table I) are indicated by small and large dashed circles. (b) $P2_1nm$ ZP structure (Table II). Directions of transverse displacements of Mn ions from their ideal perovskite positions are indicated by arrows. Labels on ions refer to Tables I–III.

potential energy surface. A further energy minimization was performed using $P12_11$ symmetry and 100% HF exchange. The screw axis parallel to the **b** axis naturally incorporates transverse Mn displacements found in experiment. All Hessian matrix eigenvalues were positive for this ZP CO structure and it was lower in energy than the other structures ($P11m$+7 meV/Mn ion; $P2_1nm$+14 meV/Mn ion). A structure optimization with 60% HF exchange and $Pn2_1m$ symmetry resulted in a stable CB CO structure which was 31 meV/Mn ion lower than the optimized structure with $P112_1/m$ symmetry. Fractional coordinates for the lowest energy CB and ZP CO structures found, which have $Pn2_1m$ symmetry, are given in Table I. Fractional coordinates for the $La_{0.5}Ca_{0.5}MnO_3$ ZP CO structure are compared to those determined by neutron scattering for $Pr_{0.60}Ca_{0.40}MnO_3$ (Ref. 15) in Table II.

Figure 1(a) shows atomic positions for nearly coplanar Mn and O ions projected onto the **ab** plane in the $Pn2_1m$ energy minimized structure. Positions of ions in the ZP CO structure are indicated by shaded or filled circles and positions of ions in the CB CO structure are indicated by dashed lines (Table I). The structures are coincident at the Mn1 ion positions and so this figure facilitates comparison of distortions in the **ab** plane. The main differences in ion position occur at the Mn2 and O3 positions to accommodate the switch between ZP and CO JT distortion patterns. Transverse wavelike modulations of Mn and O ion positions about ideal perovskite positions can be identified in Fig. 1(a). Modulations of either ion type have wavelength equivalent to the unit cell dimension along the **b** axis and are out of phase by $\pi/2$ and are similar to modulations of MnO_6 proposed in manganites with $x>0.5$ (Ref. 5) and $x<0.5$ (Ref. 27).

Positions of ions in the energy minimized $P2_1nm$ structure with ZP CO are shown in Fig. 1(b). The main differences in atomic positions in the plane between this ZP CO structure and the $Pn2_1m$ ZP CO structure occur at the O2 and O3 positions. Fractional coordinates for the $P2_1nm$ structures for both $La_{0.5}Ca_{0.5}MnO_3$ (this work) and for $Pr_{0.60}Ca_{0.40}MnO_3$ (Ref. 15) are compared in Table II and the

TABLE I. Fractional coordinates for $La_{0.5}Ca_{0.5}MnO_3$ with $Pn2_1m$ symmetry from *ab initio* total energy minimization. Wyckoff positions are given in the second column. Coordinates on the left-hand side were determined using a UHF calculation and those on the right-hand side using 60% HF exchange. Both structures have the (x,y) coordinates of the Mn1 ion in common.

		100%			60%		
Atom	Wyckoff	x	y	z	x	y	z
Ca1	2*a*	0.4773	0.8866	0.0000	0.4861	0.8866	0.0000
La2	2*a*	0.4652	0.3732	0.0000	0.4514	0.3673	0.0000
La3	2*a*	0.9760	0.1226	0.5000	0.9743	0.1261	0.5000
Ca4	2*a*	0.9789	0.5985	0.5000	0.9779	0.6057	0.5000
Mn1	4*b*	0.0000	0.8746	0.2445	0.0000	0.8713	0.2478
Mn2	4*b*	0.4578	0.6224	0.2534	0.4811	0.6231	0.2535
O1	4*b*	0.2463	0.0069	0.2109	0.2352	0.9977	0.2109
O2	4*b*	0.2556	0.7600	0.2112	0.2676	0.7600	0.2144
O3	4*b*	0.1813	0.2315	0.2042	0.2118	0.2433	0.2146
O4	4*b*	0.7479	0.9891	0.2753	0.7539	0.9970	0.2717
O1′	2*a*	0.4298	0.1255	0.5000	0.4320	0.1055	0.5000
O2′	2*a*	0.5550	0.1309	0.0000	0.5430	0.1337	0.0000
O3′	2*a*	0.0443	0.3645	0.5000	0.0316	0.3611	0.5000
O4′	2*a*	0.9054	0.3770	0.0000	0.9012	0.3625	0.0000

TABLE II. Fractional coordinates for $La_{0.5}Ca_{0.5}MnO_3$ (LCMO) from *ab initio* UHF energy minimization and for $Pr_{0.60}Ca_{0.40}MnO_3$ (PCMO) from single crystal neutron diffraction (Ref. 15), both with $P2_1nm$ symmetry. Wyckoff positions are given in the second column.

		LCMO			PCMO		
Atom	Wyckoff	*x*	*y*	*z*	*x*	*y*	*z*
Ca1	2*a*	0.4769	0.9021	0.0000	0.5121	0.8936	0.0000
La2	2*a*	0.4783	0.3723	0.5000	0.4784	0.3614	0.5000
La3	2*a*	0.9832	0.1286	0.0000	0.9977	0.1426	0.0000
Ca4	2*a*	0.9741	0.6093	0.5000	0.9905	0.6088	0.5000
Mn1	4*b*	0.0000	0.8743	0.2498	0.0000	0.8756	0.2489
Mn2	4*b*	0.9611	0.3775	0.7518	0.9795	0.3746	0.7492
O1	4*b*	0.2717	0.9980	0.2768	0.3044	0.9845	0.2861
O2	4*b*	0.6918	0.2685	0.7837	0.7090	0.2676	0.7891
O3	4*b*	0.1818	0.2261	0.7029	0.2112	0.2328	0.7148
O4	4*b*	0.7324	0.5211	0.2276	0.7515	0.5191	0.2110
O1′	2*a*	0.4344	0.1246	0.0000	0.4353	0.1125	0.0000
O2′	2*a*	0.5575	0.1322	0.5000	0.5743	0.1321	0.5000
O3′	2*a*	0.0375	0.3644	0.0000	0.0562	0.3758	0.0000
O4′	2*a*	0.9247	0.3777	0.5000	0.9104	0.3846	0.5000

agreement is remarkable. The starting guess for the $La_{0.5}Ca_{0.5}MnO_3$ structure in *ab initio* calculations was not the $Pr_{0.60}Ca_{0.40}MnO_3$ structure and the coordinates obtained via *ab initio* calculations are not simply a relaxation of the $Pr_{0.60}Ca_{0.40}MnO_3$ structure. There are bonds of intermediate length along the ZP axis ranging from 1.99 to 2.09 Å in *ab initio* calculations and from 1.98 to 2.05 Å in experiment[15] (Table III). Bond valence sums[29] (calculated using R_0 and B values of 1.750 and 0.37 for all Mn-O bonds) for the ZP structures are close to 3.5 in both computed and experimental ZP structures, which is indicative of an intermediate valence. The Mn-O$^-$-Mn bond angle is 160° or less in both $La_{0.5}Ca_{0.5}MnO_3$ and $Pr_{0.60}Ca_{0.40}MnO_3$.

The spin density and charge density difference of the ZP CO structure are shown in Fig. 2. Charge density difference plots are generated by subtracting densities of isolated O^{2-} and Mn^{4+} ions from the total charge density of the crystal structures and therefore show deformations of charge density at O ion sites and e_g orbital order at Mn ion sites. Each Mn ion in the ZP CO state has a d^4 configuration, O$^-$ ions order

TABLE III. Selected bond distances in Å, bond angles for LCMO from *ab initio* energy minimization and for PCMO from single crystal neutron diffraction (Ref. 15) and bond valence sums (BVS). Ion labels refer to atomic positions given in Fig. 1. The bond angle given is the Mn1*a*-O3*a*-Mn2 angle at the center of the ZP or adjacent to a JT distorted Mn ion. The structure and space group are indicated at the top of each column.

Bond	CB[a]	ZP[b]	Bond	ZP[c]	ZP[d]
Mn1*a*-O1*a*	1.92	1.99	Mn1*a*-O1*a*	2.01	2.05
Mn1*a*-O4	1.86	1.87	Mn1*a*-O1*b*	1.86	1.88
Mn1*a*-O2	1.91	1.89	Mn1*a*-O2	1.91	1.91
Mn1*a*-O3*a*	1.84	2.05	Mn1*a*-O3*a*	2.08	1.98
Mn2-O2	1.91	1.89	Mn2*a*-O2	1.90	1.90
Mn2-O3*a*	2.14	2.09	Mn2*a*-O3*a*	2.09	2.01
Mn2*s*-O1*a*	1.92	1.86	Mn2*a*-O4	1.88	1.90
Mn2-O4*a*	2.15	2.03	Mn2*a*-O4*a*	2.02	2.03
Bond angle	160	155		151	159
BVS Mn1	3.28	3.60		3.60	3.5[d]
BVS Mn2	4.08	3.56		3.53	3.5[d]

[a]$La_{0.5}Ca_{0.5}MnO_2$ $Pn2_1m$ symmetry, 60% HF exchange.
[b]$La_{0.5}Ca_{0.5}MnO_3$ $Pn2_1m$ symmetry, UHF.
[c]$La_{0.5}Ca_{0.5}MnO_3$ $P2_1nm$ symmetry, UHF.
[d]$Pr_{0.60}Ca_{0.40}MnO_3$ $P2_1nm$ symmetry, expt. (Ref. 15).

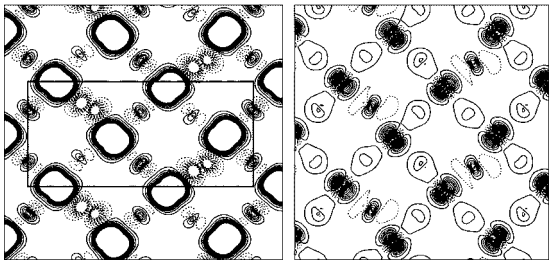

FIG. 2. Spin density and charge density difference for $La_{0.5}Ca_{0.5}MnO_3$ in the ZP state with A-type magnetic order and $Pn2_1m$ symmetry obtained using a UHF wave function. (Left-hand side) Spin density. The unit cell shown in Fig. 1(a) is outlined. (Right-hand side) Charge density difference.

in $Mn(d^4)$-O^--$Mn(d^4)$ dimers (Zener polarons) in **ab** planes and the magnetic ground state is A type.[12] UHF calculations[12] predict a magnetic moment of $0.7\mu_B$ on the O^- ion in the center of each ZP, which is opposed to the moments of neighboring ZP Mn ions. On the other hand, cluster configuration interaction (CI) calculations[16,17] show that the moment on O^- ions is much less than $0.7\mu_B$ and that orbital ordering is strongly influenced by the Madelung field of the cluster. Cluster CI calculations by the present author[17] show that the charge on these ions, measured by the Mulliken population, is approximately $-1.0e$, in agreement with UHF calculations and that the ZP are strongly bound in a FM state. In both UHF and CI calculations the total magnetic moment on each ZP is $7/2\mu_B$ in agreement with experiment.[7] The reason for the discrepancy between spin distributions in CI and UHF calculations is simply that the UHF spin function for the Mn-O^- bond is $\alpha\beta$ whereas it should be $(\alpha\beta-\beta\alpha)/\sqrt{2}$. $d_{3x^2-r^2}$ and $d_{3y^2-r^2}$ orbital order in the ZP state can clearly be seen in Fig. 2 in both spin density and charge density difference plots.

Bond lengths, the Mn1a-O3a-Mn2 bond angle and bond valence sums for the CB state with $Pn2_1m$ symmetry are given on the left-hand side of Table III. Spin densities and charge density differences are given in Fig. 3. The ground state magnetic order for the CB CO state is CE type, the magnetic order found experimentally in $La_{0.5}Ca_{0.5}MnO_3$,[2] and it consists of zig-zag FM chains as shown in Fig. 3. Mn1 ions in the chains have short (1.85 Å) Mn-O bonds while JT distorted Mn2 ions have long Mn-O bonds (2.15 Å). These are, respectively, the lengths of Mn-O bonds in $CaMnO_3$ and $LaMnO_3$.[10,30] The magnetic moments on these ions are $3.23\mu_B$ (Mn1) and $3.85\mu_B$ (Mn2) and bond valence sums are 3.28 and 4.08. All of these are characteristic of conventional CO, although charges on Mn ions as measured by Mulliken populations are essentially identical, with values of +2.02 (Mn1) and +2.02 (Mn2). A small difference in Mn ion charge has been noted in several experimental papers[19,20] in apparently CO states. A recent neutron powder diffraction study of $La_{0.5}Ca_{0.5}MnO_3$ found a pattern of bond lengths for the LT-M′ model[22] similar to the pattern found here for the CB CO state.

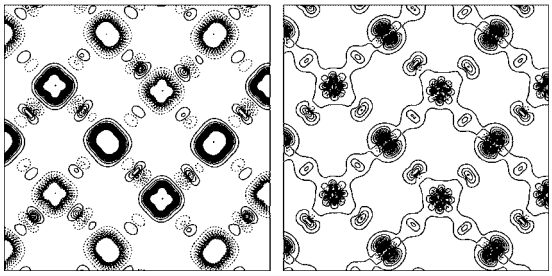

FIG. 3. Spin density and charge density difference for $La_{0.5}Ca_{0.5}MnO_3$ in the checkerboard state with CE-type magnetic order and $Pn2_1m$ symmetry obtained using 60% HF exchange. (Left-hand side) Spin density. (Right-hand side) Charge density difference.

HF and density functional methods frequently predict properties of materials (such as bond lengths or the band gap[31]) which lie either side of the experimentally observed values. Hence hybrid approaches, such as the 60% HF exchange method used here, may be expected to yield improved predictions for materials' properties. They are beginning to be used for calculating oxide electronic structures[32–34] and yield band gaps in agreement with experiment.[34] They resemble the well-known GW approximation;[35] in hybrid methods the percentage of HF exchange is reduced and replaced by a density functional exchange correlation potential while in the GW approximation, HF exchange is reduced by dynamic screening.

In summary, we have shown that the equilibrium structure for $La_{0.5}Ca_{0.5}MnO_3$ which is predicted by hybrid HF/density functional theory depends on the percentage of HF exchange used in the calculation. The CB CO state consists of FM zig-zag chains in which corner (Mn1) ions have short bonds (1.85 Å) while JT distorted (Mn2) ions have long bonds (2.15 Å) to neighboring O ions. A preliminary calculation of the RXD spectrum using this structure is in reasonably good agreement with experimental RXD spectra for $Pr_{0.60}Ca_{0.40}MnO_3$.[36] The ZP CO state consists of FM planes tiled with polarons which have Mn-O bonds of intermediate length along the polaron axis and this structure is in reasonable agreement with that found for $Pr_{0.60}Ca_{0.40}MnO_3$ by neutron scattering.[15] Transformation from the CB to the ZP state requires rehybridization at Mn1 and O3 sites together with relatively minor displacements shown in Fig. 1(a). Effective magnetic moments from magnetic susceptibility data for at least two mixed valence manganites display marked increases in effective magnetic moment on cooling below the CO transition temperature to 6.1 (Ref. 37) or $7.9\mu_B$ (Ref. 15). These magnitudes are similar to the ZP magnetic moment of $7\mu_B$. Dimerization of CE zig-zag chains to form a ZP state may produce this large effective moment.

ACKNOWLEDGMENTS

This work was supported by the Irish Higher Education Authority under the PRTLI-IITAC2 program. The author wishes to acknowledge discussions with P.G. Radaelli, A. Daoud-Aladine, and S. Grenier.

[1] C. H. Chen and S.-W. Cheong, Phys. Rev. Lett. **76**, 4042 (1996).
[2] P. G. Radaelli, D. E. Cox, M. Marezio, and S.-W. Cheong, Phys. Rev. B **55**, 3015 (1997).
[3] P. G. Radaelli, D. E. Cox, L. Capogna, S.-W. Cheong, and M. Marezio, Phys. Rev. B **59**, 14440 (1999).
[4] J. Q. Li, C. Q. Jin, and H. B. Zhao, Phys. Rev. B **64**, 020405(R) (2001).
[5] T. Nagai, T. Kimura, A. Yamazaki, T. Asaka, K. Kimoto, Y. Tokura, and Y. Matsui, Phys. Rev. B **65**, 060405(R) (2002).
[6] R. Kajimoto, H. Yoshizawa, Y. Tomioka, and Y. Tokura, Phys. Rev. B **66**, 180402(R) (2002).
[7] J. C. Loudon, N. D. Mathur, and P. A. Midgley, Nature (London) **420**, 797 (2002).
[8] M. Pissas and G. Kallias, Phys. Rev. B **68**, 134414 (2003).
[9] J. C. Loudon, S. Cox, A. J. Williams, J. P. Attfield, P. B. Littlewood, P. A. Midgley, and N. D. Mathur, Phys. Rev. Lett. **94**, 097202 (2005).
[10] E. O. Wollan and W. C. Koehler, Phys. Rev. **100**, 545 (1955).
[11] J. B. Goodenough, Phys. Rev. **100**, 564 (1955).
[12] G. Zheng and C. H. Patterson, Phys. Rev. B **67**, 220404(R) (2003).
[13] V. Ferrari, M. Towler, and P. B. Littlewood, Phys. Rev. Lett. **91**, 227202 (2003).
[14] D. J. García, K. Hallberg, C. D. Batista, M. Avignon, and B. Alascio, Phys. Rev. Lett. **85**, 3720 (2000).
[15] A. Daoud-Aladine, J. Rodriguez-Carvajal, L. Pinsard-Gaudart, M. T. Fernandez-Diaz, and A. Revcolevschi, Phys. Rev. Lett. **89**, 097205 (2002).
[16] C. de Graaf, C. Sousa, and R. Broer, Phys. Rev. B **70**, 235104 (2004).
[17] C. H. Patterson, Mol. Phys. **103**, 2507 (2005).
[18] D. V. Efremov, J. van der Brink, and D. I. Khomskii, Nat. Mater. **3**, 853 (2004).
[19] S. Grenier *et al.*, Phys. Rev. B **69**, 134419 (2004).
[20] R. J. Goff and J. P. Attfield, Phys. Rev. B **70**, 140404(R) (2004).
[21] F. Rivadulla, E. Winkler, J. S. Zhou, and J. B. Goodenough, Phys. Rev. B **66**, 174432 (2002).
[22] E. E. Rodriguez, T. Proffen, A. Llobet, J. J. Rhyne, and J. F. Mitchell, Phys. Rev. B **71**, 104430 (2005).
[23] G. Subías, J. García, M. G. Proietti, and J. Blasco, Phys. Rev. B **56**, 8183 (1997).
[24] J. García, M. C. Sánchez, G. Subías, and J. Blasco, J. Phys.: Condens. Matter **13**, 3229 (2001).
[25] J. García, M. C. Sánchez, J. Blasco, G. Subías, and M. G. Proietti, J. Phys.: Condens. Matter **13**, 3243 (2001).
[26] C. Nelson *et al.*, Phys. Rev. B **64**, 174405 (2001).
[27] B. J. Campbell, R. Osborn, D. N. Argyriou, L. Vasiliu-Doloc, J. F. Mitchell, S. K. Sinha, U. Ruett, C. D. Ling, Z. Islam, and J. W. Lynn, Phys. Rev. B **65**, 014427 (2001).
[28] V. R. Saunders *et al.*, *Crystal03 User's Manual* (University of Torino, Torino, 2003). (www. crystal.unito.it).
[29] I. D. Brown, Acta Crystallogr., Sect. B: Struct. Sci. **48**, 553 (1992).
[30] J. Rodriguez-Carvajal, M. Hennion, F. Moussa, A. H. Moudden, L. Pinsard, and A. Revcolevschi, Phys. Rev. B **57**, R3189 (1998).
[31] S. Massidda, M. Posternak, and A. Baldereschi, Phys. Rev. B **46**, 11705 (1992).
[32] I. P. R. Moreira, F. Illas, and R. L. Martin, Phys. Rev. B **65**, 155102 (2002).
[33] Y. Noel, M. Llunell, R. Orlando, P. D'Arco, and R. Dovesi, Phys. Rev. B **66**, 214107 (2002).
[34] X. Feng and N. M. Harrison, Phys. Rev. B **70**, 092402 (2004).
[35] M. S. Hybertsen and S. G. Louie, Phys. Rev. Lett. **55**, 1418 (1985).
[36] S. Grenier (private communication).
[37] A. Prodi, E. Gilioli, A. Gauzzi, F. Licci, M. Marezio, F. Bolzoni, Q. Huang, A. Santoro, and J. W. Lynn, Nat. Mater. **3**, 48 (2004).